DSMC STUDY OF HYPERSONIC ABLATION USING SPARTA

Lennart Bott[1,a], Song Chen[2], Christian Stemmer[1]

[1]Chair of Aerodynamics and Fluid Mechanics, Technical University of Munich,
Boltzmannstr. 15, DE-85748 Garching
[2] School of General Engineering, Beihang University, 37 Xueyuan Road, CN-100191 Beijing
[a]Corresponding Author: lennart.bott@tum.de

ABSTRACT

Ablative TPSs (Thermal Protection System) are used to reduce the heat load on vehicles during atmospheric reentry. In the literature, extensive efforts were made to study ablation in the continuum regime with Navier-Stokes solvers. As for the rarefied regime in high altitudes, the continuum assumption is no longer valid and the application of DSMC (Direct Simulation Monte Carlo) becomes highly desirable. In the present work, an open-source DSMC kernel SPARTA is employed to study the surface ablation of hypersonic vehicles. The primary goal is to conduct a more realistic simulation of the ablation process by taking relevant physical factors, such as the particle kinetic energy, into consideration. For that purpose, changes to the existing kinetic energy flux ablation model were implemented. The simulation results show that the flow structures are instantaneously adapted to the ablated surfaces and that the improved model enables a better phenomenological description of the ablation process.

Index Terms— Atmospheric reentry, Hypersonic flows, Ablation, DSMC, SPARTA

1. INTRODUCTION

Due to its high reentry velocity, a vehicle is usually exposed to severe aerothermodynamic environment and a large fraction of kinetic energy is converted into heat. Ablative TPSs (Thermal Protection System) are used to protect the spacecraft by reducing the heat load through ablative processes such as vaporization, surface reactions, burning etc., which bring significant challenges to the numerical simulation. So far, a lot of efforts have been devoted to simulate these phenomena in the continuum gas regime with Navier-Stokes solvers [1, 2].

However, this approach may no longer be valid for the rarefied regime in high altitudes, especially for Knudsen numbers larger than 0.01. Under rarefied conditions, particle-based methods such as DSMC (Direct Simulation Monte Carlo) can deliver more accurate results [3]. DSMC was developed by G. A. Bird in the 1970s and is a probabilistic method which is based on the Boltzmann equations [4].

In the present work, two-dimensional surface ablation of an isothermal circle and square during hypersonic nonequilibrium flows is studied with an open-source DSMC kernel SPARTA (Stochastic PArallel Rarefied-gas Time-accurate Analyzer) [5]. The primary focus of this study is to investigate the ablation model of DSMC for hypersonic flows and to improve the simulation performance of the SPARTA code. To accomplish this, modifications to the existing kinetic energy flux ablation rule were implemented and a scaling factor was introduced. Hereby, it should be noted that specific material ablation rates are not taken into account. Instead, this work focuses on studying general ablation principles. The remainder of the paper is arranged as follows. In Sec. 2, the numerical method, the relevant parts of the source code and the corresponding changes are presented. The simulation results are then discussed in Sec. 3 and finally the conclusions are drawn in Sec. 4.

2. METHODOLOGY

The SPARTA code is primarily developed by Sandia National Laboratories. It provides an interface to perform DSMC simulations of low-density gases in two or three dimensions. It is easily extendable and is designed to allow the implementation of new features and functions to the code. It also includes MPI (Message Passing Interface) that enables high performance parallel computing [6].

2.1. Ablation in SPARTA

In October 2019, commands to perform ablation and for this purpose implicit surfaces were added by S. J. Plimpton *et al.* [5] to the SPARTA source code. Implicit surface data is stored for each individual grid cell in grid corner point values. As SPARTA uses a two- or three-dimensional hierarchical Cartesian grid, depending on the dimensionality of the calculation, there are four or eight grid corner point values per cell, respectively. Each one of them has values in between 0 and 255. For two-dimensional calculations, a Marching Square algorithm is then used to determine the surface element in each grid cell by finding the right combination of grid corner

point values in a library [7, 8]. Thereby, the case that all grid corner point values are 0 or 255 would correspond to a cell without any surface element or to a completely filled cell, respectively.

Ablation is performed in cycles and is based on a predefined ablation rule such as counting the particle-surface collisions or calculating the kinetic energy flux for each cell for a certain number of timesteps (samples). At the end of each ablation cycle, the grid corner point values are reduced depending on the calculated and averaged value of the ablation rule. The smallest grid corner point value of each cell is reduced first until it is zero. Subsequently, the next smaller value is reduced until all the grid corner point values in a cell are zero. Consequently, the surface in the cell got completely "ablated". After each ablation cycle, a new surface is determined by using the Marching Square Algorithm. In this way, a receding surface can be modeled, as can be seen in figure 1 [5].

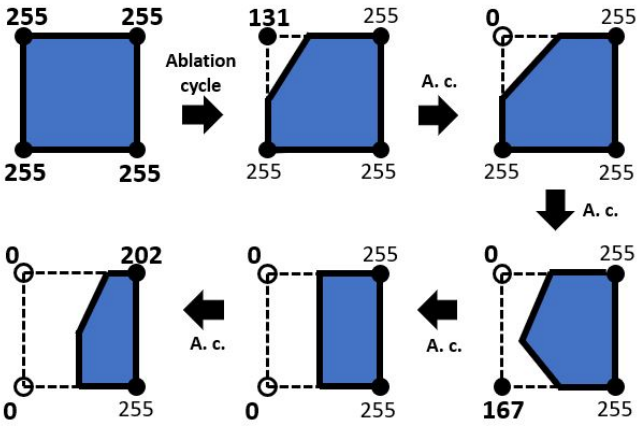

Fig. 1. Schematic of a receding surface in a two-dimensional grid cell due to multiple ablation cycles

2.2. Kinetic energy flux ablation rule

The kinetic energy flux ablation rule was added with the complete ablation model to the source code by S. J. Plimpton *et al.* [5] and is briefly presented in this section. As DSMC is a particle based method, the kinetic energy flux ablation rule is calculated via the particle properties. The model provides options to account for surface reactions. In the present study for simplification, no surface reactions are taken into account and the impacting particles are just "reflected" on the surface. Thus, one particle has the same mass before and after the collision. For every particle-surface collision, the transferred kinetic energy E_{kin} to the surface is calculated:

$$E_{kin} = \frac{1}{2}\, m\, (v_{pre}^2 - v_{post}^2), \tag{1}$$

where m is the particle mass, v_{pre} is the particle velocity before the collision:

$$v_{pre} = ||\overrightarrow{v_{pre}}||, \tag{2}$$

and v_{post} is the assigned particle velocity after a diffuse surface-collision which is derived from a surface-temperature-dependent Gaussian distribution.

Then, the particle flux $E_{kin,flux}$ on a surface element A in a cell per length of a timestep dt is:

$$E_{kin,flux} = E_{kin}\, \frac{f_{num}}{A\, dt}, \tag{3}$$

where f_{num} is the ratio between the number of real to simulated particles:

$$f_{num} = \frac{\#\ real\ particles}{\#\ simulated\ particles}. \tag{4}$$

Due to the stochastic nature of the DSMC method, it is necessary to determine an average value for $E_{kin,flux}$ for each cell and ablation cycle. Multiple iterations (samples) are executed and $E_{kin,flux}$ of each particle-surface collision in a cell is summed up and then divided by the number of samples n_{sample}:

$$\overline{E}_{kin,flux} = \frac{\Sigma\, E_{kin,flux}}{n_{sample}}. \tag{5}$$

Hereby, one should not confuse that n_{sample} is not equal to the number of particle-surface collisions in one cell. It is the number of how many timesteps dt are taken into account to calculate the average value, as it is possible to have multiple or zero collisions during one timestep.

The value of $\overline{E}_{kin,flux}$ for each cell is then deducted from the grid corner point values of the particular cell.

2.3. Modification of the ablation rule

Two issues were addressed to extend and improve the kinetic energy flux ablation rule. Firstly, it was found that the assigned particle velocity after a diffuse surface collision v_{post} negatively influences the value of the ablation rule $\overline{E}_{kin,flux}$. As v_{post} is derived from a surface-temperature-dependent Gaussian distribution, v_{post} increases for a higher surface temperature. As one can imagine for an adiabatic surface, the most aerothermodynamically stressed parts of the surface are hottest and should therefore also ablate fastest. However, as can be seen in equation 1, a larger v_{post} leads to a smaller $\overline{E}_{kin,flux}$. Thus, the ablation of the hot surface parts is performed slower as it should for such a thermally stressed surface. Consequently, this leads to an inaccurate depiction of the ablation process of the whole body.

Also for an isothermal wall, v_{post} can create inaccuracies especially in the case of wrong assumptions for v_{pre} or the surface temperature. For instance, if the surface temperature is overestimated in comparison to the particle velocity near

the wall, $\overline{E}_{kin,flux}$ would become negative and the surface would not be ablated even though there are particle-surface collisions.

In the present study, this issue is solved by simply neglecting the kinetic energy flux of the reflected particles. Instead, we focus on the impinging particles and only the impacting kinetic energy flux is taken into account for the calculation of $\overline{E}_{kin,flux}$. It should be noted that the particles are still assigned a v_{post} from the surface-temperature-dependent Gaussian distribution.

Secondly, it was discovered that $\overline{E}_{kin,flux}$ has unreasonably high values especially under atmospheric reentry conditions in high altitudes. As the maximum value to be deducted from a cell is 1020 (four times 255), one ablation cycle is then sufficient to completely ablate the surface in a cell. This process can be considered as independent from the actual kinetic energy of the impacting particles because also rather slow particles still have a sufficiently large kinetic energy to completely ablate a cell.

Additionally, $\overline{E}_{kin,flux}$ is calculated for each cell exclusively and the remaining value of $\overline{E}_{kin,flux}$ after a complete ablation of a cell is not transferred to the adjacent cells. Hence, they are not further ablated and a part of $\overline{E}_{kin,flux}$ is not used to perform ablation and is lost. To ensure that a cell is not completely ablated in one ablation cycle, a scaling factor α was implemented to restrict $\overline{E}_{kin,flux}$ from reaching for the ablation performance critical values:

$$\alpha = \frac{f_{num}}{A_{cell}\, dt}\, E_{kin,max}, \tag{6}$$

where f_{num} and dt are the same as in equation 3, $E_{kin,max}$ is the maximal kinetic energy of a particle and A_{cell} is a grid-size-based assumption of the length of the surface in a cell (A two-dimensional surface is a line):

$$A_{cell} = \frac{dx + dy}{2}. \tag{7}$$

Here, dx and dy are the length of a grid cell in x- and y-direction, respectively. The maximal kinetic energy of a particle is defined as:

$$E_{kin,max} = \frac{1}{2}\, m\, v_{pre,max}^2, \tag{8}$$

where m is the particle mass and $v_{pre,max}$ is the maximal velocity of a particle before hitting the surface:

$$v_{pre,max} = ||\overrightarrow{v}|| + v_{therm}. \tag{9}$$

$v_{pre,max}$ is composed of the argument of the three-dimensional velocity vector $\overrightarrow{v}$ and the thermal velocity of the particle v_{therm}:

$$v_{therm} = \sqrt{\frac{3\, k_B\, T}{m}}, \tag{10}$$

where k_B is the Boltzmann constant and T is the particle temperature. Thus, the scaled ablation rule is:

$$\overline{E}_{kin,flux,\alpha} = \frac{\overline{E}_{kin,flux}}{\alpha}. \tag{11}$$

2.4. Simulation parameters

A circle and square with a diameter or side length of $0.5\ m$ are observed, respectively. As implicit surfaces are used, the size of the geometry is coupled to the size and number of grid cells. Here, the grid cell size is $0.0025\ m$. Hence, the circle and the square have a diameter or length of 200 grid cells, respectively. Generally, the more grid cells are used to create a geometry, the higher resolution is obtained. However, the computational cost also increases significantly.

The surface is modeled as an isothermal, non-catalytic wall with a constant temperature of $1000\ K$. Furthermore, a diffuse particle reflection model without surface reactions is used. The main free stream properties are shown in table 1 and were taken from Thomas J. Scanlon *et al.* [9]. They correspond to a typical reentry trajectory at an altitude of 86 km and a Mach number of 24.85. The particle mixture consists of 79 % N_2 and 21 % O_2 and the effects of energy relaxation are not taken into account.

Table 1. Free stream conditions

Parameters	Value	Description
ρ	$1.433 \cdot 10^{20}$	Number density $[1/m^3]$
T	187	Particle temperature $[K]$
v	6813	Stream velocity $[m/s]$
Ma	24.85	Mach number

The main DSMC parameters are listed in table 2. The number of samples per ablation cycle n_{sample} is one of the main parameters that define the accuracy of $\overline{E}_{kin,flux}$ for each cell and ablation cycle. The scaling factor α is calculated with the set of equations in subsection 2.3.

Table 2. DSMC parameters

Parameters	Value	Description
dx, dy	0.0025	Grid cell size $[m]$
dt	$4 \cdot 10^{-7}$	Length of a timestep $[s]$
n_{sample}	100	Number of samples
f_{num}	$4.478 \cdot 10^{13}$	See equation 4
α	$2.07 \cdot 10^{-5}$	Scaling factor

3. RESULTS AND DISCUSSION

The ablation process of the circle and square are shown in figure 2 and 3, respectively. The DSMC simulation particles of N_2 (red) and O_2 (green) are injected on the left side of the calculation domain. Consequently, the flow is from left to right. For both figures, (I) is modeled with the previous ablation rule for the kinetic energy flux and (II) with the modified ablation rule (see subsection 2.3). To assure a comparability between (I) and (II), all calculations were executed with the same parameters. However, for (I) significantly less ablation cycles take place because the values for $\overline{E}_{kin,flux}$ are much larger and thus the material is ablated much faster.

(I) Previous results

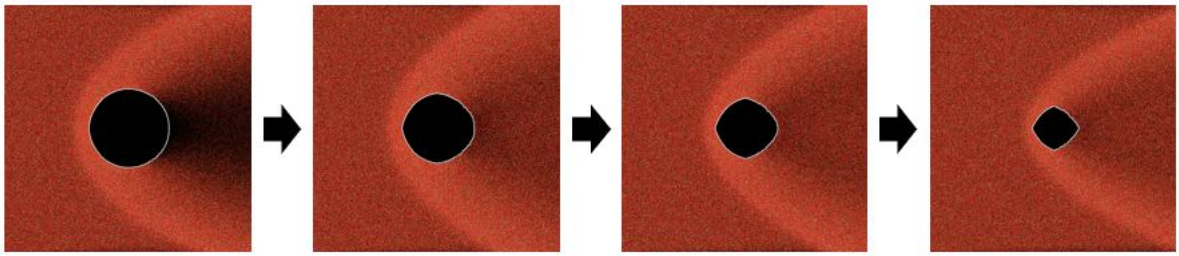

(II) Present results

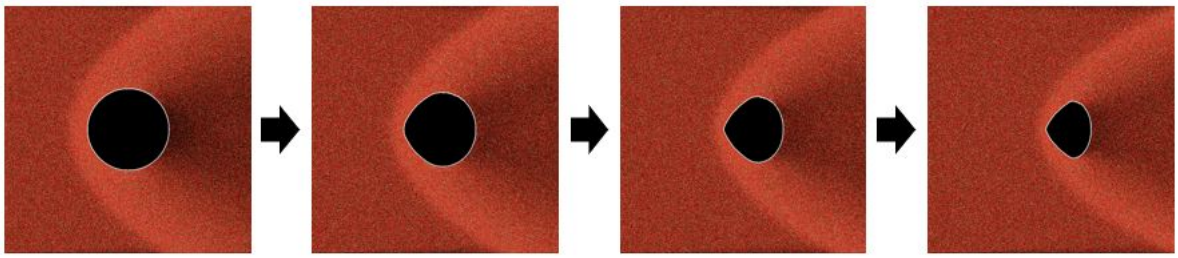

Fig. 2. Comparison of the ablation process of a circle with the previous **(I)** and present altered kinetic energy flux ablation rule with scaling factor **(II)**

(I) Previous results

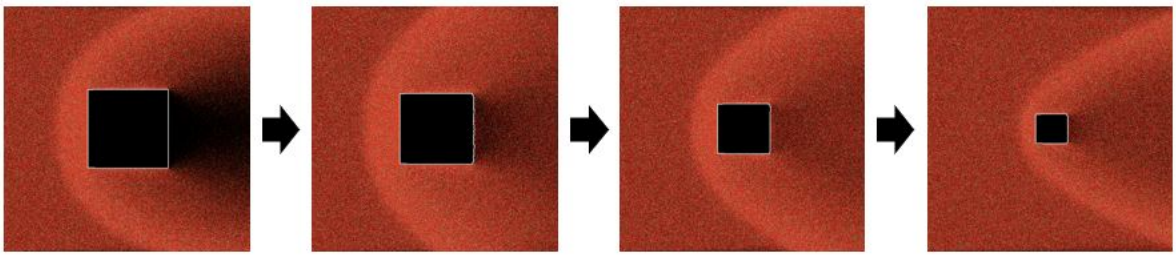

(II) Present results

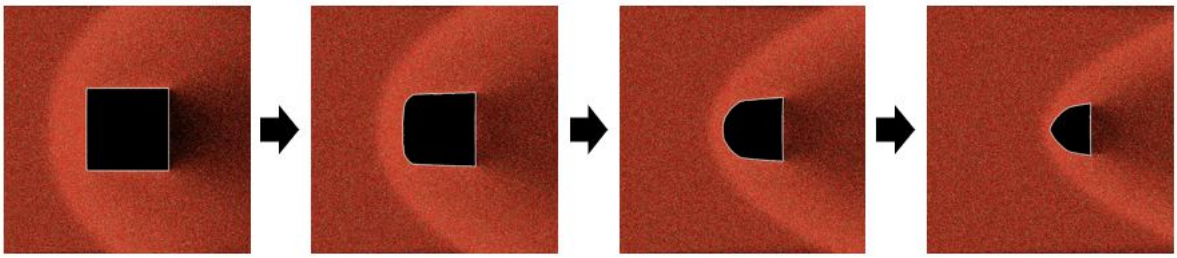

Fig. 3. Comparison of the ablation process of a square with the previous **(I)** and present altered kinetic energy flux ablation rule with scaling factor **(II)**

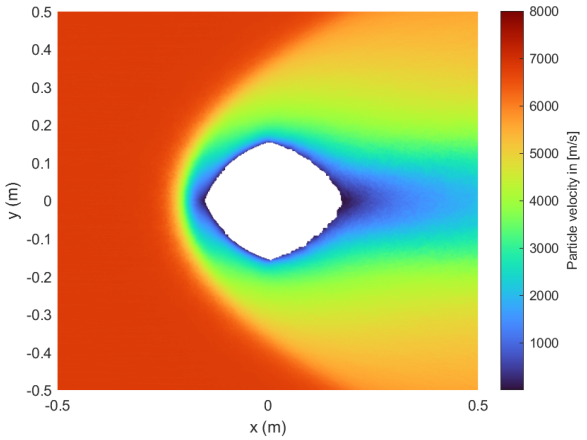

Circle after multiple ablation cycles

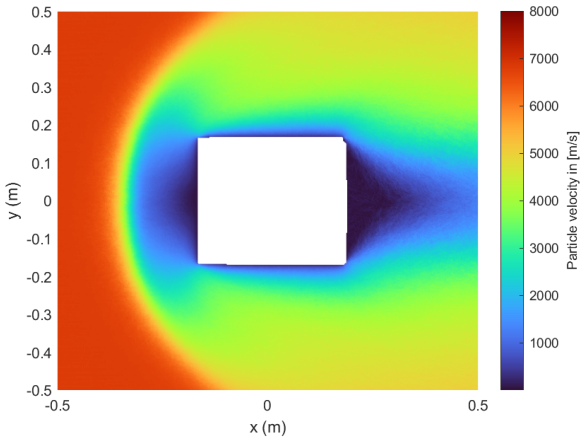

Square after multiple ablation cycles

Fig. 4. Particle velocity field for previous results **(I)**

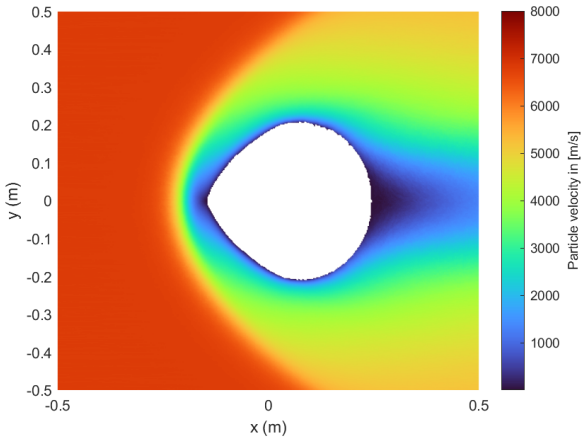

Circle after multiple ablation cycles

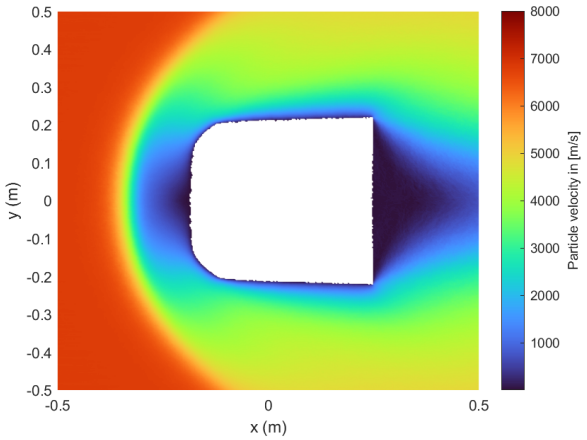

Square after multiple ablation cycles

Fig. 5. Particle velocity field for present results **(II)**

For each calculation, the creation of a shock wave can be observed as well as an instantaneous adaptation of the flow structures to the ablated surface. However, noticeable differences in the ablation process between (I) and (II) for the circle and the square can be seen. For the circle, the ablation process of (I) leads to a diamond-shaped geometry with corners on the top and bottom. This is due to the high values of $\overline{E}_{kin,flux}$ even for rather "slow" particles in the wake region of the circle. Consequently, the particles hitting the back side of the geometry will also completely ablate the material in a cell. As the ablation rule is calculated per cell and the remaining value of $\overline{E}_{kin,flux}$ is not transferred to adjacent cells, the same number of grid cells is ablated per ablation cycle from the front and back side of the geometry, which leads to its diamond shape.

This effect is even more visible for the ablation process of the square. As can be seen in (I) of figure 3, the square is equally ablated from each of its four sides. Consequently, its quadratic shape remains unaltered during the whole ablation process. However, as can be seen in figure 4, the particle velocity is much smaller in the wake region of the square than at its leading edge. This should lead to a much slower ablation of the back compared to the front side of the square. Additionally, due to the increasing particle velocities from the stagnation point to the corners, the values for $\overline{E}_{kin,flux}$ should increase and the leading edge corners should be ablated first. Thus, for (I) variations of the kinetic energy of the particles seem to have only a limited effect on the ablation of the geometry.

The modified ablation rule (II) leads to more physical sound results. Here the circle is ablated into an arrow-shaped geometry with much less material being ablated on the back than at the front side (see (II) figure 2). Furthermore, the velocity dependency of the ablation rule is visible. As can be seen in figure 5, the particle velocity is much smaller around the stagnation point and increases towards the top and bottom

of the circle. Hence, less material is ablated in the stagnation point than downstream of it, leading to the arrow-shaped geometry. Additionally, the slow ablation at the back of the circle is in accordance to the slow particle velocities in the wake region.

The velocity field around the square (see figure 5) shows lower particle velocities at the stagnation point and in the wake region than at its leading edge corners. The square is ablated in agreement to the velocity field with the leading edge corners of the square being ablated first while less material is ablated at the stagnation point (see (II) figure 3). Consequently, the leading edge is ablated into a circular shape. Furthermore, the top and bottom edges of the square become inclined towards the leading edge. Then, similar to the ablation of the circle, the ablation continuously forms an arrow-shaped geometry. Additionally, the back side of the square is hardly ablated which again confirms the dependency of the ablation intensity on the particle velocity.

4. CONCLUSION

The hypersonic ablation phenomena was modeled in DSMC based on the kinetic energy of the particles using SPARTA. For the previous model, it was found that the flow structures are instantaneously adapted to the ablated surface. However, some issues were discovered which lead to inaccuracies in the depiction of a physical sound ablation process. Modifications to the existing model were implemented, evaluated and compared to the results of the previous ablation rule. The changes to the model resolved those issues and showed significant improvements for the simulation of ablation. Future work will be devoted to further enhance the simulation accuracy and to the inclusion of surface reactions as well as material properties.

5. ACKNOWLEDGEMENT

The authors gratefully acknowledge the Humboldt-foundation for funding this project and the computational and data resources provided by the Leibniz Supercomputing Centre (www.lrz.de).

6. REFERENCES

[1] Y.-K. Chen and F. S. Milos, "Navier-Stokes solutions with finite rate ablation for planetary mission earth reentries," *Journal of Spacecrafts and Rockets*, vol. 42, no. 6, pp. 961–970, December 2005.

[2] D. Bianchi, F. Nasuti and E. Martelli, "Navier-Stokes simulations of hypersonic flows with coupled graphite ablation," *Journal of Spacecrafts and Rockets*, vol. 47, no. 4, pp. 554–562, August 2010.

[3] I. D. Boyd and T. E. Schwartzentruber, "Nonequilibrium gasdynamics and molecular simulation," Cambridge University Press, April 2017, ISBN: 9781139683494.

[4] G. Bird, "Molecular gas dynamics and the direct simulation of gas flows," Oxford University Press, 1994, ISBN: 9780198561958.

[5] S. J. Plimpton, S. G. Moore and A. Borner, "Direct Simulation Monte Carlo on petaflop supercomputers and beyond," *Physics of Fluids*, vol. 31, no. 086101, August 2019.

[6] M. A. Gallis, J. R. Torczynski, S. J. Plimpton, D. J. Rader and T. Koehler, "Direct Simulation Monte Carlo: The quest for speed," *AIP Conference Proceedings 1628*, pp. 27–36, December 2014.

[7] W. E. Lorensen and H. E. Cline, "Marching Cubes: A high resolution 3d surface construction algorithm," *Computer Graphics*, vol. 21, no. 4, 1987.

[8] C. Maple, "Geometric design and space planning using the Marching Squares and Marching Cube algorithms," *International Conference on Geometric Modeling and Graphics, Proceedings*, pp. 90–95, 2003.

[9] T. J. Scanlon, C. White, M. K. Borg, R. C. Palharini, E. Farbar, I. D. Boyd, J. M. Reese and R. E. Brown, "Open-source Direct Simulation Monte Carlo chemistry modeling for hypersonic flows," *AIAA Journal*, vol. 53, no. 6, pp. 1670–1680, June 2015.